

Estimating Reflectance Layer from A Single Image: Integrating Reflectance Guidance and Shadow/Specular Aware Learning

Yeying Jin,¹ Ruoteng Li,^{1,2} Wenhan Yang,³ Robby T. Tan,^{1,4}

¹ National University of Singapore, Singapore

² ByteDance, Singapore

³ Peng Cheng Laboratory, China

⁴ Yale-NUS College, Singapore

{jinyeying, liruoteng}@u.nus.edu, yangwh@pcl.ac.cn, robby.tan@nus.edu.sg

Abstract

Estimating reflectance layer from a single image is a challenging task. It becomes more challenging when the input image contains shadows or specular highlights, which often render an inaccurate estimate of the reflectance layer. Therefore, we propose a two-stage learning method, including reflectance guidance and a Shadow/Specular-Aware (S-Aware) network to tackle the problem. In the first stage, an initial reflectance layer free from shadows and specularities is obtained with the constraint of novel losses that are guided by prior-based shadow-free and specular-free images. To further enforce the reflectance layer to be independent from shadows and specularities in the second-stage refinement, we introduce an S-Aware network that distinguishes the reflectance image from the input image. Our network employs a classifier to categorize shadow/shadow-free, specular/specular-free classes, enabling the activation features to function as attention maps that focus on shadow/specular regions. Our quantitative and qualitative evaluations show that our method outperforms the state-of-the-art methods in the reflectance layer estimation that is free from shadows and specularities.

1 Introduction

Reflectance layer estimation is a fundamental task in computer vision. It is a part of intrinsic image decomposition, which decomposes an input image into the reflectance layer and the shading layer (Barrow et al. 1978). The reflectance layer provides useful information for real-world applications, *e.g.*, surface retexturing (Garces et al. 2012), relighting (Liu et al. 2020a), object compositing (Bi, Han, and Yu 2015). Unfortunately, reflectance layer estimation from a single image is an inherently ill-posed problem.

Several methods have been proposed to deal with the problem. Non-deep learning methods *e.g.*, (Bell, Bala, and Snavely 2014) impose priors on the estimated reflectance layer. Supervised learning methods *e.g.*, (Das, Karaoglu, and Gevers 2022), while effective, still suffer from problems, particularly those related to shadows and specularities. Some existing unsupervised learning methods learn from time-lapse data (Li and Snavely 2018b; Liu et al. 2020a), multi-view data (Yi, Tan, and Lin 2020) or sets of unpaired images (Liu et al. 2020b).

Copyright © 2023, Association for the Advancement of Artificial Intelligence (www.aaai.org). All rights reserved.

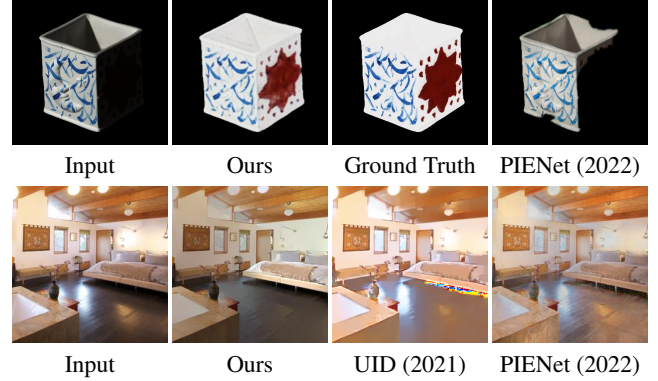


Figure 1. Comparison between our results and the state-of-the-art methods UIDNet (Zhang et al. 2021) and PIENet (Das, Karaoglu, and Gevers 2022). Unlike existing methods, our method estimates the reflectance layer free from shadows and specularities.

Among these methods, only few consider shadows (Baslamisli et al. 2021a,b) and specular highlights (Yi, Tan, and Lin 2020). However, they suffer from a few drawbacks. First, most of them are trained only on synthesized datasets, and thus their accuracy depends heavily on the quality of the synthesized data. Second, while these methods work well in some cases, they tend to fail in handling large shadow or specular regions, as shown in Fig. 1. Third, most of these methods assume that reflectance changes cause abrupt image intensity changes, while shading changes cause smooth image intensity changes (Land and McCann 1971). However, shadows, which should belong to the shading layer, can also cause abrupt intensity changes in the real world, which goes against this assumption.

In this paper, our goal is to decompose a diffuse reflectance layer that is free from shadows and specularities. To achieve this, we introduce a two-stage network based on reflectance guidance and a Shadow/Specular-Aware (S-Aware) network. The first stage is to obtain an initial diffuse reflectance layer free from shadows and specularities. To achieve this, we introduce novel losses constrained by prior-based shadow-free (Finlayson, Drew, and Lu 2004) and specular-free images (Tan and Ikeuchi 2005).

Once the initial reflectance layer is obtained, we feed it into the S-Aware network, which identifies shadow/specular regions by modulating the activation features as attention maps. To enable the S-Aware network to self-learn the shadow/specular regions, a Shadow/Specularity Classifier (S-Classifier) is employed to distinguish the first-stage estimated reflectance layer from the input image. Specifically, by distinguishing shadows from shadow-free or specularities from specular-free, the activation features form shadow/specular attention. Our attention mechanism modulates the activation weights with encoded features that capture spatially varying regions. Once our network can focus on shadow/specular regions, it can refine the reflectance layer to be free from shadows and specularities. In summary, here are our contributions:

- To the best of our knowledge, our method is the first single-image diffuse reflectance layer estimation network that performs robustly even in the presence of shadows and specularities. This differs from existing intrinsic image decomposition methods, which tend to fail to remove shadows and specularities from the reflectance layer.
- We introduce a reflectance guidance framework that provides reliable guidance for our network to learn the reflectance layer. Our novel losses constrain the reflectance layer free from shadows and specularities, based on prior-based shadow-free and specular-free images.
- We propose an S-Aware network to modulate activation features as shadow/specular attention. Our network automatically learns to focus on these regions, since our S-Classifier distinguishes shadows from shadow-free or specularities from specular-free.

Our quantitative and qualitative evaluations show that our method outperforms the state-of-the-art methods in various datasets for suppressing shadows and specularities in the reflectance layer, including: 4 intrinsic datasets, 2 shadow datasets and 1 specular dataset.

2 Related Work

Reflectance Layer Estimation The Retinex algorithm (Land and McCann 1971) assumes reflectance changes cause large gradients, while shading variation corresponds to small gradients. Subsequently, various priors, *e.g.*, sparse reflectance (Shen and Yeo 2011), reflectance colors (Ye et al. 2014), textures (Zhao et al. 2012), depth (Lee et al. 2012) are utilized to regularize the reflectance layer. However, with only hand-crafted constraints, these methods are not adaptive enough, and scene-specific parameters are hard to cover real-world shadows and specularities. Moreover, the assumption that shading changes cause smooth image intensity changes is not likely to cover the large shading change, such as shadow regions.

In recent years, many deep-learning-based methods have been introduced (Garces et al. 2022), and most of them adopt supervised learning (Narihira, Maire, and Yu 2015; Baslamisli, Le, and Gevers 2018; Fan et al. 2018; Das, Karaoglu, and Gevers 2022). The challenge of applying learning-based methods is the lack of a variety of real im-

ages with ground truth. Synthetic datasets *e.g.*, (Butler et al. 2012; Shi et al. 2017; Li and Snavely 2018a; Baslamisli et al. 2021a) highly depend on the quality of the rendering techniques and 3D models. Poor rendering quality will make the network fail to handle real images in the testing stage, due to the gaps between the synthetic and real image domains.

Real image datasets *e.g.*, (Grosse et al. 2009; Bell, Bala, and Snavely 2014; Kovacs et al. 2017)) are either too limited, lack diversity, or have highly sparse annotations. To address the limitations of supervised learning methods, a few unsupervised learning methods are proposed. They mainly focus on images with static reflectance and varied illumination (Lettry, Vanhoey, and Van Gool 2018; Ma et al. 2018; Li and Snavely 2018b; Liu et al. 2020a). Unlike multi-image approaches, unpaired translation (Liu et al. 2020b) and internal self-similarity (Zhang et al. 2021) provide more solutions. However, most existing methods have artefacts in the reflectance layer, particularly on the shadow and specular regions. Unlike existing methods, our network estimates the reflectance layer that is free from shadows and specularities.

Shadow and Specularity Removal A few intrinsic image decomposition methods (Baslamisli et al. 2021b,a; Zhang et al. 2021) attempt to address shadows, and other methods (Shi et al. 2017; Yi, Tan, and Lin 2020; Li et al. 2020) attempt to solve specular highlights separation using a large-scale synthetic data in training. However, the accuracy of the rendering limits the performance of the methods on the real-world shadows and specularities.

Note that, there are a few shadow/specularity removal methods that do not decompose the input image to the intrinsic layers, such as (Kawakami, Ikeuchi, and Tan 2005; Jin, Sharma, and Tan 2021)) for shadow removal, and (Tan and Ikeuchi 2005; Yang, Wang, and Ahuja 2010; Shen and Zheng 2013; Guo, Zhou, and Wang 2018) for specularity removal. While these methods work to some extent, the problems of shadow/specular removal are still open problems.

3 Proposed Method

Fig. 2 shows our pipeline to estimate the reflectance layer that is free from shadows/specularities. First, we obtain the initial reflectance layer by employing reflectance guidance, and then refine the reflectance layer using the Shadow/Specular-Aware (S-Aware) network.

3.1 Intrinsic Image Reflectance Guidance

We estimate the reflectance layer \mathbf{R} , given an input image \mathbf{I} and governed by $\mathbf{I} = \mathbf{R} \odot \mathbf{S}$, where \odot is the element-wise multiplication. \mathbf{S} is the shading layer. Note that, shadows naturally belong to the shading layer, as they are phenomena caused by light (instead of by objects). While specularities are caused by surface reflectance (Nayar et al. 1991; Tan 2021), and thus should belong to the reflectance layer. However, many applications assume diffuse only reflectance, and hence the reflectance layer that is independent from specularities is more desirable. Therefore, given an input image, our goal is to obtain the diffuse reflectance layer that is free from both shadows and specular highlights. Throughout this paper, reflectance layer refers to the diffuse reflectance layer.

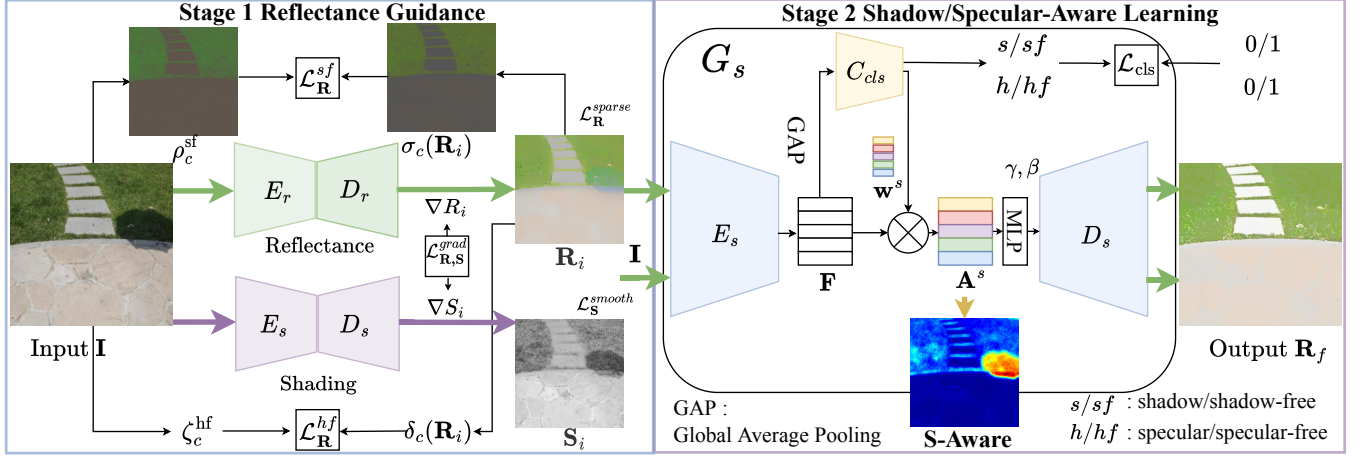


Figure 2. Our framework consists of two stages: reflectance guidance and Shadow/Specular-Aware (S-Aware). In the first stage, to obtain the initial reflectance layer \mathbf{R}_i , we propose the novel shadow-free \mathcal{L}_R^{sf} (see Fig. 3) and specular-free \mathcal{L}_R^{hf} losses (see Fig. 4). In the second stage, the initial reflectance layer and the input image are fed to the S-Aware network to obtain the final reflectance output \mathbf{R}_f . Our S-Aware network is represented by G_s (contain an S-Classifier C_{cls}). By distinguishing shadows from shadow-free, or specularities from specular-free, our network automatically learns the activation weights \mathbf{w}^s . Multiplying \mathbf{w}^s to modulate the encoded features \mathbf{F} , obtain S-Aware attention \mathbf{A}^s , which focuses on shadow/specular regions.

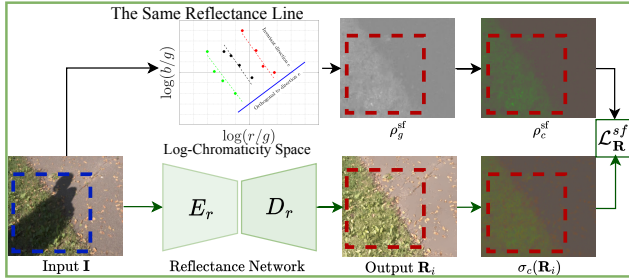


Figure 3. Using the shadow-free loss \mathcal{L}_R^{sf} , our first stage reflectance network learns to remove shadows in the reflectance layer \mathbf{R}_i . Shadow-free image ρ_c^{sf} do not have shadow regions (see the red dashed rectangles).

We employ encoder-decoder (E_r - D_r and E_s - D_s , with subscript r, s stands for reflectance, shading) to simultaneously decompose the input image \mathbf{I} into an initial reflectance layer \mathbf{R}_i and an initial shading layer \mathbf{S}_i , as shown in Fig. 2.

Due to the ill-posed nature of our problem, we propose to utilize the shadow-free image (Finlayson, Drew, and Lu 2004) and the specular-free image (Tan and Ikeuchi 2005) as priors to guide the first stage decomposition network. For this guidance, we propose two novel losses: shadow-free loss \mathcal{L}_R^{sf} and specular-free loss \mathcal{L}_R^{hf} .

Shadow-Free Loss To obtain a shadow-free reflectance layer, we compute a shadow-free image in the log-chromaticity space (Finlayson, Drew, and Lu 2009). In this space, pixels belonging to the same reflectance surface form a single line, where the line is dependent on light colors (implying that shadow and non-shadow pixels of the same reflectance will lie on the same line). Entropy minimiza-

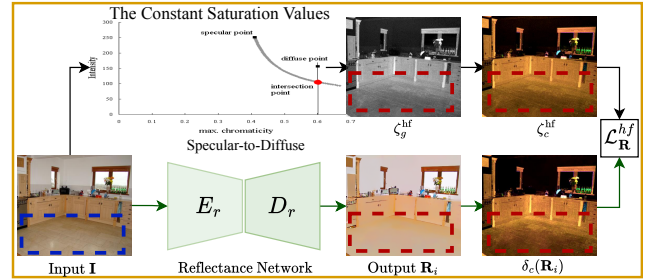


Figure 4. Using the specular-free loss \mathcal{L}_R^{hf} , our first stage reflectance network learns to remove specularities in the reflectance layer \mathbf{R}_i . Specular-free image ζ_c^{hf} is free from specularities (see the red dashed rectangles).

tion can capture this line and generate a grayscale image free from shadows (Fig. 5b). Then, we compute a colored shadow-free image, ρ_c^{sf} , by instilling the illumination colors back (Drew, Finlayson, and Hordley 2003) (Fig. 5c).

Guided by the colored shadow-free image, ρ_c^{sf} , our reflectance network learns to obtain the shadow-free reflectance layer through the shadow-free loss, defined as:

$$\mathcal{L}_R^{sf} = |\sigma_c(\mathbf{R}_i) - \rho_c^{sf}|_1, \quad (1)$$

where σ_c is the chromaticity, $\sigma_c(\mathbf{x}) = \frac{I_c(\mathbf{x})}{I_r(\mathbf{x}) + I_g(\mathbf{x}) + I_b(\mathbf{x})}$, $c \in \{r, g, b\}$ represents each RGB color channel.

Specular-Free Loss Tan and Ikeuchi (Tan and Ikeuchi 2005) define a specular-free image as an image that has an identical geometric profile to the diffuse component of the input image yet has different hue values. The key idea in obtaining the specular-free image is to force the saturation values to be constant for all pixels regardless of whether they

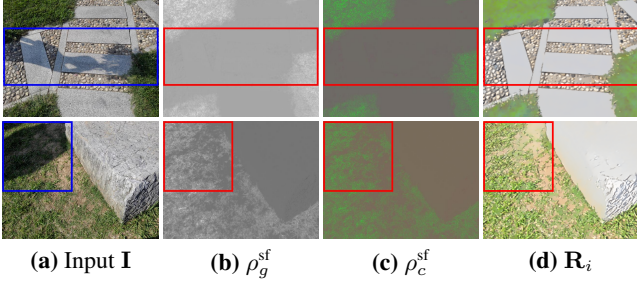


Figure 5. (a) Input image with shadows. (b) The grayscale shadow-free image, and (c) The colored shadow-free image ρ_c^{sf} do not have shadows (see the red boxes), providing prior guidance to our network. Therefore, our reflectance network learns to obtain (d) the shadow-free reflectance layer \mathbf{R}_i .

are affected by specularities or not (Tan and Ikeuchi 2005; Li, Tan, and Cheong 2018). These constant saturation values make specular highlights disappear from the image.

Fig. 6 shows some examples of specular-free images. The specularities are removed in the grayscale specular-free images (second row) and the colored specular-free images ζ_c^{hf} (bottom row). Guided by the colored specular-free image, the reflectance network learns to obtain the specular-free reflectance layer through the specular-free loss, defined as:

$$\mathcal{L}_{\mathbf{R}}^{\text{hf}} = \|\delta_c(\mathbf{R}_i) - \zeta_c^{\text{hf}}\|_1, \quad (2)$$

where δ_c is the transformation from RGB to the colored specular-free images.

Gradient Separation Loss Since reflectance gradients $\nabla \mathbf{R}_i$ are sparse in the gradient domain, while shading gradients $\nabla \mathbf{S}_i$ are smooth (Bonneel et al. 2014) in the intensity domain, to separate the two uncorrelated layers, we use the gradient separation loss (Zhang, Ng, and Chen 2018):

$$\mathcal{L}_{\mathbf{R}, \mathbf{S}}^{\text{grad}} = \sum_{n=1}^3 \|\tanh(\lambda_{\mathbf{R}} \|\nabla \mathbf{R}_i^{\downarrow n}\|) \odot \tanh(\lambda_{\mathbf{S}} \|\nabla \mathbf{S}_i^{\downarrow n}\|)\|_F,$$

where $\|\cdot\|_F$ is the Frobenius norm, \odot is the Hadamard multiplication. $\mathbf{R}_i^{\downarrow n}$ and $\mathbf{S}_i^{\downarrow n}$ represent \mathbf{R}_i and \mathbf{S}_i downsampled by a factor of 2^{n-1} , $n = 3$, using bilinear interpolation, the parameters $\lambda_{\mathbf{R}} = \sqrt{\|\nabla \mathbf{S}_i^{\downarrow n}\|_F / \|\nabla \mathbf{R}_i^{\downarrow n}\|_F}$, $\lambda_{\mathbf{L}} = \sqrt{\|\nabla \mathbf{R}_i^{\downarrow n}\|_F / \|\nabla \mathbf{S}_i^{\downarrow n}\|_F}$ are normalization factors to balance gradient magnitudes of the reflectance layer and the shading layer.

Shading Smooth Loss To impose smooth constraints on the shading layer, we employ a smooth loss that computes the horizontal and vertical gradients:

$$\mathcal{L}_{\mathbf{S}}^{\text{smooth}} = \|\nabla(\mathbf{S}_i)\|_1. \quad (3)$$

Reflectance Sparse Gradient Loss Unlike the shading layer, the gradients of the reflectance layer are sparse (Land

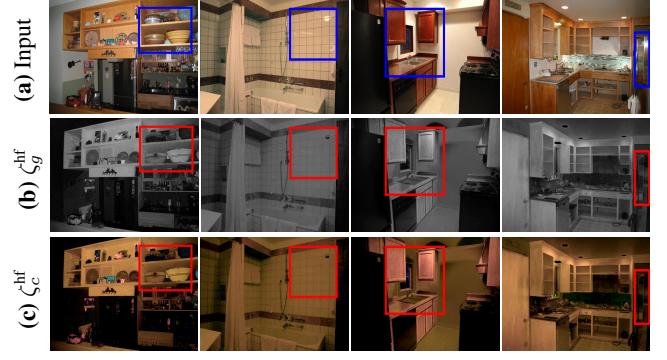


Figure 6. (a) Input image with specularities, (b) The grayscale specular-free image, and (c) The colored specular-free image ζ_c^{hf} . The specularities are reduced in the specular-free images (see the red boxes), providing prior guidance to our reflectance network.

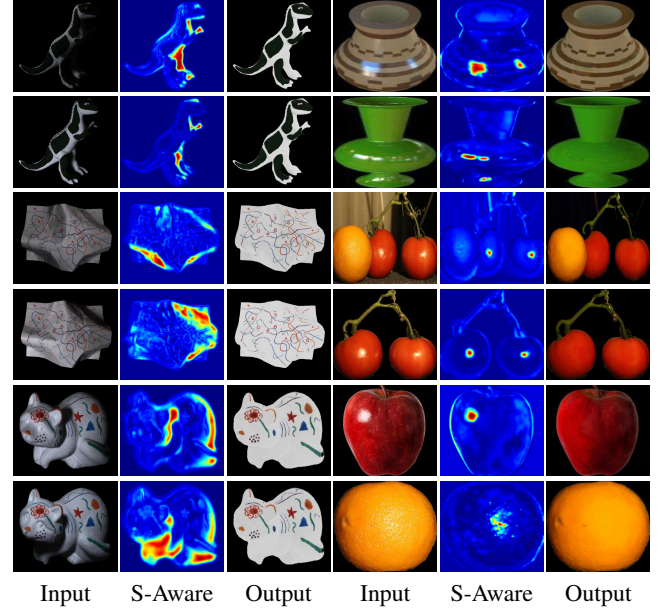


Figure 7. Left-most three columns are the real images from the MIT dataset (Grosse et al. 2009). The right-most three columns are the images from the real highlight (Yi, Tan, and Lin 2020) and synthetic ShapeNet dataset (Chang et al. 2015). Our S-Aware network focuses on shadow/specular regions, which are the modulated activation features.

and McCann 1971). To pursue this, we develop a regularization term made by the reweighted l_p norm (Emmanuel J. Candès 2008) to punish the gradients:

$$\mathcal{L}_{\mathbf{R}}^{\text{sparse}} = \omega \|\nabla(\mathbf{R}_i)\|_1; \quad \omega = \frac{1}{\|\nabla(\mathbf{R}_i)\|^{1-p} + \epsilon} \quad (4)$$

where ϵ is a small positive number that stabilizes the numerical calculation, p is a parameter that determines the extent of the sparsity, $p = 0.5$, and ω is regarded as a constant that is not involved in the back-propagation optimization.

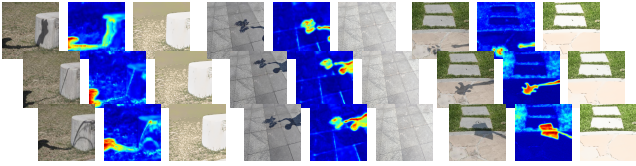


Figure 8. Our S-Aware network can capture spatially varying regions from dataset (Qu et al. 2017; Wang, Li, and Yang 2018), the diffuse reflectance of the objects in the static scene always remains the same.

We multiply each of the above-mentioned loss functions with its respective weight, where in our experiments, we empirically set $\lambda_{\mathbf{R}}^{\text{sf}}$, $\lambda_{\mathbf{R}}^{\text{hf}}$, $\lambda_{\mathbf{R},\mathbf{S}}^{\text{grad}}$ to 1, since they are in the same scale. We also empirically set $\lambda_{\mathbf{S}}^{\text{smooth}} = 0.5$, $\mathcal{L}_{\mathbf{R}}^{\text{sparse}} = 0.01$.

3.2 Shadow/Specular-Aware Network

To further refine the reflectance layer, in the second stage, our S-Aware network focuses on shadow/specular regions. As shown in Fig. 2, the architecture of the S-Aware network is represented by G_s (the subscript s stands for shadow/specular). It has an encoder E_s , a decoder D_s , and a shadow/specularity classifier (S-Classifier) C_{cls} . The input to the S-Aware network is the initial reflectance layer \mathbf{R}_i and the original input image \mathbf{I} . The output is the refined reflectance image \mathbf{R}_f , which is our final output.

We train our S-Classifier to predict the two-category classification probability and to judge whether the encoded features come from a certain class. The classification’s confidence score is the likelihood of the input image belonging to the shadow/shadow-free or specular/specular-free classes. To be more specific, the encoder E_s generates the encoded features \mathbf{F} . Inspired by the class activation mapping (Zhou et al. 2016; Kim et al. 2019; Jin, Yang, and Tan 2022), we multiply the features with classification weights \mathbf{w}^s , learned by our S-Classifier. Then, we obtain the shadow/specular-activated features, denoted as \mathbf{A}^s , defined as:

$$\mathbf{A}^s = \frac{1}{m} \sum_{i=1}^m \mathbf{w}_i^s \mathbf{F}_i, \quad (5)$$

where m is the total number of feature maps. The activated features indicate the importance of the regions to distinguish the shadows from shadow-free, or specularities from specular-free. The S-Classifier C_{cls} performs a two-category classification, in which the loss is based on the following equation:

$$\mathcal{L}_{\text{cls}} = -(\mathbb{E}[\log(C_{\text{cls}}(\mathbf{I}))] + \mathbb{E}[\log(1 - C_{\text{cls}}(\mathbf{R}_i))]). \quad (6)$$

For this classification task, the activated features generate a form of attention that focuses on the shadow/specular regions, as shown in Fig. 7 and Fig. 8.

Spatially Varying Regions In a spatially varying dataset shown in Fig. 8, the shadow/specular regions of the scenes constantly change, while the diffuse reflectance of the objects in the static scene always remains the same. To help our network focus on the large shadow/specular regions in

the spatially varying dataset to remove them, we use feature statistics and the normalization layer to capture the spatial-variant property of shadows/specularities. Since the mean and variance of the features encode the statistics of an image, aligning them implies transferring the style of the image.

Instance Normalization (IN) (Huang and Belongie 2017) is used in unsupervised style transfer (Liu et al. 2020b): $\phi^c = \frac{\phi - \mu^c(\phi)}{\sqrt{\sigma^c(\phi)^2 + \epsilon}}$, where μ^c and σ^c are the channel-wise mean and standard deviation, and ϕ is the activation of the previous convolutional layer. Unlike IN, layer normalization (LN) (Ba, Kiros, and Hinton 2016) captures the average and variance of each pixel among a batch of input data: $\phi^l = \frac{\phi - \mu^l(\phi)}{\sqrt{\sigma^l(\phi)^2 + \epsilon}}$, where μ^l and σ^l are the layer-wise mean and the standard deviation. Our S-Aware network dynamically adjusts the ratio ν (where $\nu \in \{0, 1\}$) between IN and LN operations: $\text{LIN}(\gamma, \beta, \nu) = \gamma((1 - \nu) \cdot \phi^c + \nu \cdot \phi^l) + \beta$, where γ and β are parameters generated by the fully connected layer. ϕ^c , ϕ^l are the channel-wise, layer-wise normalization functions, respectively.

Adversarial and Translation Losses Our S-Aware network, G_s , is coupled with a discriminator D_{sf} . We use the least-square GAN (LSGAN) (Mao et al. 2017) adversarial losses to stabilize our network training:

$$\mathcal{L}_{\text{adv}}(G_s, D_{sf}) = \mathbb{E}[(D_{sf}(\mathbf{I}) - 1)^2] + \mathbb{E}[(D_{sf}(\mathbf{R}_f))^2].$$

When the S-Aware network, G_s , takes the original input, it outputs the reflectance layer. We enforce the following loss:

$$\mathcal{L}_{\text{trans}}(G_s) = \|\mathbf{G}_s(\mathbf{I}) - \mathbf{R}_f\|_1. \quad (7)$$

Diffuse Loss We learn the reflectance layer also from the diffuse reflection component \mathbf{I}_d , where $\mathbf{I}_d = \mathbf{R}_d \odot \mathbf{S}$ with \mathbf{R}_d is the true diffuse reflectance layer. For images suffered only from shadows, the diffuse reflection component is the image itself, where $\mathbf{I}_d = \mathbf{I}$. For images suffered from specular highlights, the diffuse reflection component can be computed: $\mathbf{I}_d = \mathbf{I} - \mathbf{I}_s$ (Shafer 1985; Tan and Ikeuchi 2005), where \mathbf{I}_s is the specular reflection component. Some real (Yi, Tan, and Lin 2020) and synthetic datasets (Shi et al. 2017) provide the information of the diffuse reflection component and the corresponding image together, which can be used in our training. Hence, we define our diffuse loss as:

$$\mathcal{L}_{\text{diff}}(G_s) = \|\mathbf{R}_f \odot \mathbf{S}_i - \mathbf{I}_d\|_1. \quad (8)$$

Overall Loss We multiply each loss function with its respective weight, and sum them together to obtain our overall loss function. The weights of the losses, \mathcal{L}_{cls} , \mathcal{L}_{adv} , $\mathcal{L}_{\text{trans}}$ are empirically set to 5, 1, 5 in our experiments. The weights of $\mathcal{L}_{\text{diff}}$ are 1, since they are in the same scale.

4 Experimental Results

Reflectance Layer Estimation on Shadows To evaluate our method, we use 2 real (MIT Intrinsic, IIW) and 2 synthetic intrinsic image decomposition datasets (MPI-Sintel, ShapeNet), and 2 shadow datasets (SRD, USR). Fig. 9 and

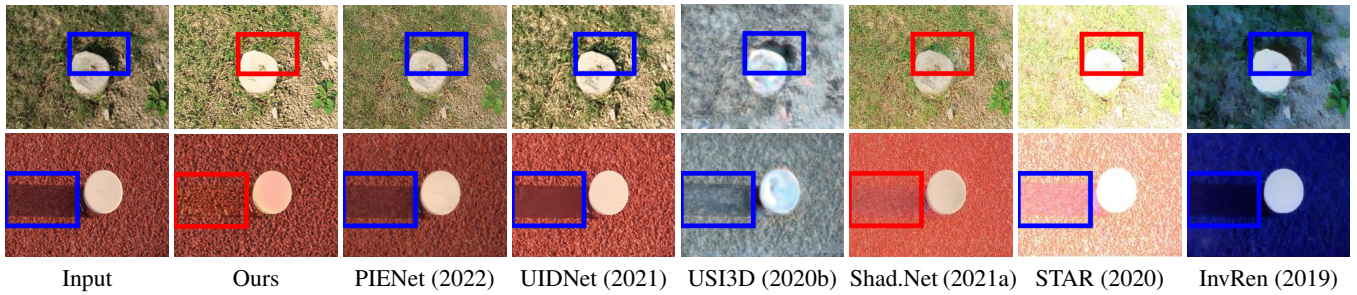


Figure 9. Comparing results on the shadow dataset (Hu et al. 2019). Most existing methods perform poorly in separating out shadows from the reflectance layer, while our method more effectively estimates the reflectance layer that is free from shadows.

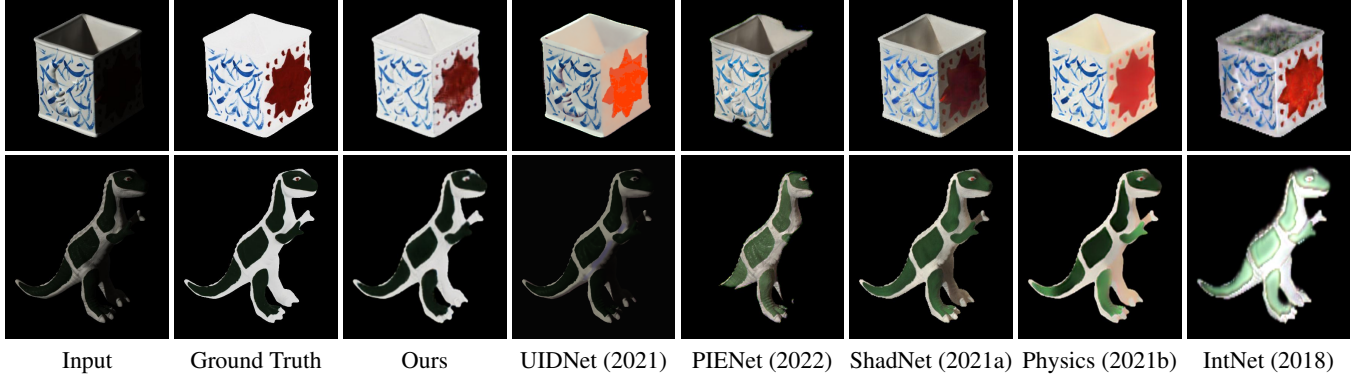


Figure 10. Comparing results on the MIT dataset (Grosse et al. 2009). Most existing methods perform poorly in separating out shadows from the reflectance layer, while our method more effectively estimates the reflectance layer that is free from shadows.

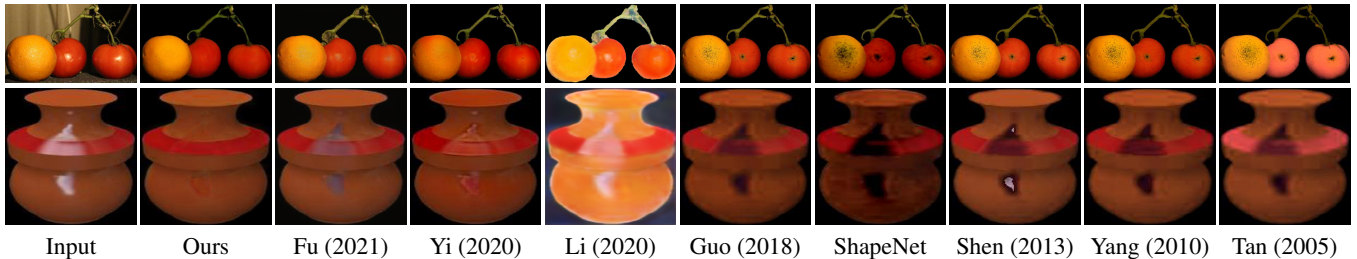


Figure 11. Comparing results on the real highlight dataset (Yi, Tan, and Lin 2020) and synthetic specular ShapeNet dataset (Shi et al. 2017). Existing methods perform poorly in separating specularities from the reflectance layer.

Fig. 10 show our results on the real image USR shadow (Hu et al. 2019) and MIT Intrinsic dataset (Grosse et al. 2009). Fig. 12 shows our results on the synthetic datasets MPI-Sintel (Butler et al. 2012) and ShapeNet (Chang et al. 2015). Most SOTA methods perform poorly in separating shadows from the reflectance layer. When the images have shadow regions, these methods cannot estimate the information under the shadow regions. Our results are free from shadows.

We make a fair comparison with SOTA intrinsic image decomposition methods: PIENet (Das, Karaoglu, and Gevers 2022), UIDNet (Zhang et al. 2021), ShadingNet (Baslamisli et al. 2021a), Physics (Baslamisli et al. 2021b), USI3D (Liu et al. 2020b); optimization-based method: STAR (Xu et al. 2020), inverse rendering method: InverseRenNet (Yu and

Smith 2019), etc.

Reflectance Layer Estimation on Specularities To evaluate our method, we use 1 synthetic intrinsic image decomposition dataset and 1 real specular dataset. Fig. 11 shows our results on real (Yi, Tan, and Lin 2020) and synthetic specular ShapeNet (Shi et al. 2017) datasets. Our method estimates the reflectance layer more effectively, in particular for the specular regions, while others may fail to recover some parts of the specular regions, leaving black artefacts in the specular/saturated regions. Our supplementary material describes datasets in detail including the number of training, testing, augmenting, etc.

To fairly compare to specular methods, we include learning-based intrinsic image decomposition methods:

Methods	Training set	WHDR%↓
STAR (2020)	—	32.90
IIW (2014)	—	20.64
ShapeNet (2017)	ShapeNet (2.5M)	59.40
IntrinsicNet (2018)	ShapeNet (20K)	32.10
CGI (2018a)	SUNCG	26.10
InvRen (2019)	MegaDepth	21.40
PIE-Net (2022)	NED+IIW	18.50
Fan <i>et al.</i> (2018)* ¹	IIW	14.45
Yi (2020)	CustomerPhotos	51.10
Physics (2021b)	ShapeNet (20K)	28.90
Ma <i>et al.</i> (2018)	IIW	28.04
IIDWW (2018b)	BigTime	20.30
USI3D (2020b)	CGI+IIW	18.69
UIDNet (2021)	—	18.21
Ours	IIW	17.97

Table 1. Results for IIW dataset (Bell, Bala, and Snavely 2014) using WHDR (Bell, Bala, and Snavely 2014). * denotes use ground truth supervision in training and post-processed to benefit the WHDR score.

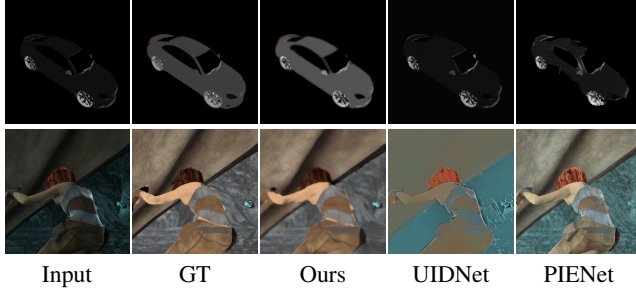


Figure 12. Comparing results on the MPI-Sintel (Butler et al. 2012) (last row) and ShapeNet intrinsic dataset (Shi et al. 2017) (first row).

Yi (Yi, Tan, and Lin 2020), ShapeNet (Shi et al. 2017), inverse rendering method: Li (Li et al. 2020), etc. We also include learning-based highlight separation method (Fu et al. 2021), optimization-based methods (Guo, Zhou, and Wang 2018; Shen and Zheng 2013; Yang, Wang, and Ahuja 2010; Tan and Ikeuchi 2005).

Quantitative Evaluation Tables 1, 2 show quantitative results on IIW and ShapeNet datasets. In Table 1, for the quantitative evaluation of reflectance images, we employ the weighted human disagreement rate (WHDR) from (Bell, Bala, and Snavely 2014). In Table 2, we employ si-MSE, si-LMSE from (Barron and Malik 2014).

Ablation Studies We conduct ablation studies to analyze the effectiveness of our first-stage reflectance layer guidance, which is shown in Fig. 13. To show the effectiveness of the first stage, we train our network without the first stage. We directly input the image to the second stage, bypassing the first stage. Table 2 shows that our first stage has a performance gain of 35% (from 0.85 to 0.63) on the

Methods	si-MSE↓			si-LMSE↓
	R	S	Avg.	Total
LM (2014)	3.38	2.96	3.17	6.23
Fan <i>et al.</i> (2018)	3.02	3.15	3.09	7.17
Ma <i>et al.</i> (2018)	2.84	2.62	2.73	5.44
USI3D (2020b)	1.85	1.08	1.47	4.65
Ours w/o stage2	1.13	2.00	1.57	4.93
Ours w/o stage1	0.85	2.17	1.51	4.85
Ours w/o S-Aware	0.79	2.05	1.42	4.15
Ours w/o \mathcal{L}_R^{sf}	0.73	2.07	1.40	4.73
Ours w/o \mathcal{L}_R^{hf}	0.66	2.04	1.35	4.19
Ours	0.63	2.00	1.31	4.14

Table 2. Results for ShapeNet intrinsic dataset (Shi et al. 2017) and the ablation studies of our method.

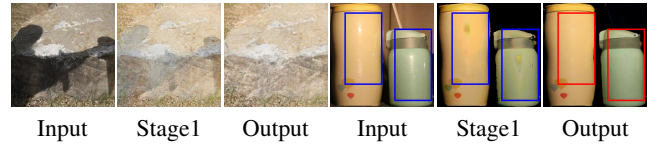


Figure 13. Ablation studies on stage-one.

ShapeNet dataset; implying our first stage provides a good initial shadow/specular-free guidance. For the first stage, we further study the effectiveness of shadow-free loss (\mathcal{L}_R^{sf}) and specular-free loss (\mathcal{L}_R^{hf}). We use shadow/specular-free images in our losses to constrain our initial estimate. We also use other losses to constrain our initial estimate. Hence, the output of our first stage can outperform specular/shadow-free images. For the second stage, we compare our results with and without S-Aware design. That means we remove the S-Classifier and the classification loss. The corresponding quantitative results are shown in Table 2.

5 Conclusion

In this paper, we have proposed a two-stage network to estimate the reflectance layer free from shadows and specularities. With the reflectance guidance and the S-Aware network, our method can robustly separate shadows and specularities out of the reflectance layer. We propose novel shadow-free and specular-free losses to estimate the initial reflectance layer. To further refine the reflectance layer, we integrate a classifier into our network, enabling our method to focus on shadow/specular regions. Experimental results have confirmed that our method is effective and outperforms the state-of-the-art reflectance layer estimation methods.

Acknowledgment

This research/project is supported by the National Research Foundation, Singapore under its AI Singapore Programme (AISG Award No: AISG2-PhD/2022-01-037[T]), and partially supported by MOE2019-T2-1-130. Robby T. Tan’s work is supported by MOE2019-T2-1-130.

References

- Ba, J. L.; Kiros, J. R.; and Hinton, G. E. 2016. Layer normalization. *arXiv preprint arXiv:1607.06450*.
- Barron, J. T.; and Malik, J. 2014. Shape, illumination, and reflectance from shading. *IEEE transactions on pattern analysis and machine intelligence*, 37(8): 1670–1687.
- Barrow, H.; Tenenbaum, J.; Hanson, A.; and Riseman, E. 1978. Recovering intrinsic scene characteristics. *Comput. Vis. Syst*, 2(3-26): 2.
- Baslamisli, A. S.; Das, P.; Le, H.-A.; Karaoglu, S.; and Gevers, T. 2021a. ShadingNet: image intrinsics by fine-grained shading decomposition. *International Journal of Computer Vision*, 1–29.
- Baslamisli, A. S.; Le, H.-A.; and Gevers, T. 2018. CNN based learning using reflection and retinex models for intrinsic image decomposition. In *Proceedings of the IEEE Conference on Computer Vision and Pattern Recognition*, 6674–6683.
- Baslamisli, A. S.; Liu, Y.; Karaoglu, S.; and Gevers, T. 2021b. Physics-based shading reconstruction for intrinsic image decomposition. *Computer Vision and Image Understanding*, 205: 103183.
- Bell, S.; Bala, K.; and Snavely, N. 2014. Intrinsic images in the wild. *ACM Transactions on Graphics (TOG)*, 33(4): 1–12.
- Bi, S.; Han, X.; and Yu, Y. 2015. An l1 image transform for edge-preserving smoothing and scene-level intrinsic decomposition. *ACM Transactions on Graphics (TOG)*, 34(4): 1–12.
- Bonneel, N.; Sunkavalli, K.; Tompkin, J.; Sun, D.; Paris, S.; and Pfister, H. 2014. Interactive intrinsic video editing. *ACM Transactions on Graphics (TOG)*, 33(6): 1–10.
- Butler, D. J.; Wulff, J.; Stanley, G. B.; and Black, M. J. 2012. A naturalistic open source movie for optical flow evaluation. In *European conference on computer vision*, 611–625. Springer.
- Chang, A. X.; Funkhouser, T.; Guibas, L.; Hanrahan, P.; Huang, Q.; Li, Z.; Savarese, S.; Savva, M.; Song, S.; Su, H.; et al. 2015. Shapenet: An information-rich 3d model repository. *arXiv preprint arXiv:1512.03012*.
- Das, P.; Karaoglu, S.; and Gevers, T. 2022. PIE-Net: Photometric Invariant Edge Guided Network for Intrinsic Image Decomposition. In *Proceedings of the IEEE/CVF Conference on Computer Vision and Pattern Recognition*, 19790–19799.
- Drew, M. S.; Finlayson, G. D.; and Hordley, S. D. 2003. Recovery of chromaticity image free from shadows via illumination invariance. In *IEEE Workshop on Color and Photometric Methods in Computer Vision, ICCV'03*, 32–39. Cite-seer.
- Emmanuel J. Candès, S. P. B., Michael B. Wakin. 2008. Enhancing Sparsity by Reweighted l_1 Minimization. *Journal of Fourier Analysis and Applications*, 14: 877–905.
- Fan, Q.; Yang, J.; Hua, G.; Chen, B.; and Wipf, D. 2018. Revisiting deep intrinsic image decompositions. In *Proceedings of the IEEE conference on computer vision and pattern recognition*, 8944–8952.
- Finlayson, G. D.; Drew, M. S.; and Lu, C. 2004. Intrinsic images by entropy minimization. In *European conference on computer vision*, 582–595.
- Finlayson, G. D.; Drew, M. S.; and Lu, C. 2009. Entropy minimization for shadow removal. *International Journal of Computer Vision*, 85(1): 35–57.
- Fu, G.; Zhang, Q.; Zhu, L.; Li, P.; and Xiao, C. 2021. A multi-task network for joint specular highlight detection and removal. In *Proceedings of the IEEE/CVF Conference on Computer Vision and Pattern Recognition*, 7752–7761.
- Garces, E.; Munoz, A.; Lopez-Moreno, J.; and Gutierrez, D. 2012. Intrinsic images by clustering. In *Computer graphics forum*, volume 31, 1415–1424. Wiley Online Library.
- Garces, E.; Rodriguez-Pardo, C.; Casas, D.; and Lopez-Moreno, J. 2022. A Survey on Intrinsic Images: Delving Deep into Lambert and Beyond. *International Journal of Computer Vision*, 130(3): 836–868.
- Grosse, R.; Johnson, M. K.; Adelson, E. H.; and Freeman, W. T. 2009. Ground truth dataset and baseline evaluations for intrinsic image algorithms. In *2009 IEEE 12th International Conference on Computer Vision*, 2335–2342. IEEE.
- Guo, J.; Zhou, Z.; and Wang, L. 2018. Single image highlight removal with a sparse and low-rank reflection model. In *Proceedings of the European Conference on Computer Vision (ECCV)*, 268–283.
- Hu, X.; Jiang, Y.; Fu, C.-W.; and Heng, P.-A. 2019. Mask-ShadowGAN: Learning to remove shadows from unpaired data. In *Proceedings of the IEEE/CVF International Conference on Computer Vision*, 2472–2481.
- Huang, X.; and Belongie, S. 2017. Arbitrary Style Transfer in Real-Time With Adaptive Instance Normalization. In *Proceedings of the IEEE International Conference on Computer Vision (ICCV)*.
- Jin, Y.; Sharma, A.; and Tan, R. T. 2021. DC-ShadowNet: Single-Image Hard and Soft Shadow Removal Using Unsupervised Domain-Classifer Guided Network. In *Proceedings of the IEEE/CVF International Conference on Computer Vision*, 5027–5036.
- Jin, Y.; Yang, W.; and Tan, R. T. 2022. Unsupervised night image enhancement: When layer decomposition meets light-effects suppression. In *European Conference on Computer Vision*, 404–421. Springer.
- Kawakami, R.; Ikeuchi, K.; and Tan, R. T. 2005. Consistent surface color for texturing large objects in outdoor scenes. In *Tenth IEEE International Conference on Computer Vision (ICCV'05) Volume 1*, volume 2, 1200–1207. IEEE.
- Kim, J.; Kim, M.; Kang, H.; and Lee, K. 2019. U-GAT-IT: unsupervised generative attentional networks with adaptive layer-instance normalization for image-to-image translation. *arXiv preprint arXiv:1907.10830*.
- Kovacs, B.; Bell, S.; Snavely, N.; and Bala, K. 2017. Shading annotations in the wild. In *Proceedings of the IEEE Conference on Computer Vision and Pattern Recognition*, 6998–7007.
- Land, E. H.; and McCann, J. J. 1971. Lightness and retinex theory. *Josa*, 61(1): 1–11.

- Lee, K. J.; Zhao, Q.; Tong, X.; Gong, M.; Izadi, S.; Lee, S. U.; Tan, P.; and Lin, S. 2012. Estimation of intrinsic image sequences from image+ depth video. In *European Conference on Computer Vision*, 327–340. Springer.
- Lettry, L.; Vanhoey, K.; and Van Gool, L. 2018. Unsupervised deep single-image intrinsic decomposition using illumination-varying image sequences. In *Computer Graphics Forum*, volume 37, 409–419. Wiley Online Library.
- Li, R.; Tan, R. T.; and Cheong, L.-F. 2018. Robust optical flow in rainy scenes. In *Proceedings of the European Conference on Computer Vision (ECCV)*, 288–304.
- Li, Y.; and Brown, M. S. 2014. Single image layer separation using relative smoothness. In *Proceedings of the IEEE Conference on Computer Vision and Pattern Recognition*, 2752–2759.
- Li, Z.; Shafiei, M.; Ramamoorthi, R.; Sunkavalli, K.; and Chandraker, M. 2020. Inverse rendering for complex indoor scenes: Shape, spatially-varying lighting and svbrdf from a single image. In *Proceedings of the IEEE/CVF Conference on Computer Vision and Pattern Recognition*, 2475–2484.
- Li, Z.; and Snavely, N. 2018a. Cgintrinsics: Better intrinsic image decomposition through physically-based rendering. In *Proceedings of the European Conference on Computer Vision (ECCV)*, 371–387.
- Li, Z.; and Snavely, N. 2018b. Learning intrinsic image decomposition from watching the world. In *Proceedings of the IEEE Conference on Computer Vision and Pattern Recognition*, 9039–9048.
- Liu, A.; Ginosar, S.; Zhou, T.; Efros, A. A.; and Snavely, N. 2020a. Learning to factorize and relight a city. In *Computer Vision–ECCV 2020: 16th European Conference, Glasgow, UK, August 23–28, 2020, Proceedings, Part IV 16*, 544–561. Springer.
- Liu, Y.; Li, Y.; You, S.; and Lu, F. 2020b. Unsupervised learning for intrinsic image decomposition from a single image. In *Proceedings of the IEEE/CVF Conference on Computer Vision and Pattern Recognition*, 3248–3257.
- Ma, W.-C.; Chu, H.; Zhou, B.; Urtasun, R.; and Torralba, A. 2018. Single image intrinsic decomposition without a single intrinsic image. In *Proceedings of the European Conference on Computer Vision (ECCV)*, 201–217.
- Mao, X.; Li, Q.; Xie, H.; Lau, R. Y.; Wang, Z.; and Paul Smolley, S. 2017. Least squares generative adversarial networks. In *Proceedings of the IEEE international conference on computer vision*, 2794–2802.
- Narihira, T.; Maire, M.; and Yu, S. X. 2015. Direct intrinsics: Learning albedo-shading decomposition by convolutional regression. In *Proceedings of the IEEE international conference on computer vision*, 2992–2992.
- Nayar, S. K.; Ikeuchi, K.; Kanade, T.; et al. 1991. Surface reflection: physical and geometrical perspectives.
- Qu, L.; Tian, J.; He, S.; Tang, Y.; and Lau, R. W. 2017. Deshadownet: A multi-context embedding deep network for shadow removal. In *Proceedings of the IEEE Conference on Computer Vision and Pattern Recognition*, 4067–4075.
- Shafer, S. A. 1985. Using color to separate reflection components. *Color Research & Application*, 10(4): 210–218.
- Shen, H.-L.; and Zheng, Z.-H. 2013. Real-time highlight removal using intensity ratio. *Applied optics*, 52(19): 4483–4493.
- Shen, L.; and Yeo, C. 2011. Intrinsic images decomposition using a local and global sparse representation of reflectance. In *CVPR 2011*, 697–704. IEEE.
- Shi, J.; Dong, Y.; Su, H.; and Yu, S. X. 2017. Learning non-lambertian object intrinsics across shapenet categories. In *Proceedings of the IEEE Conference on Computer Vision and Pattern Recognition*, 1685–1694.
- Tan, R. T. 2021. Specularity, specular reflectance. In *Computer Vision: A Reference Guide*, 1185–1188. Springer.
- Tan, R. T.; and Ikeuchi, K. 2005. Separating Reflection Components of Textured Surfaces Using a Single Image. *IEEE Trans. Pattern Anal. Mach. Intell.*, 27(2): 178–193.
- Wang, J.; Li, X.; and Yang, J. 2018. Stacked conditional generative adversarial networks for jointly learning shadow detection and shadow removal. In *Proceedings of the IEEE Conference on Computer Vision and Pattern Recognition*, 1788–1797.
- Xu, J.; Hou, Y.; Ren, D.; Liu, L.; Zhu, F.; Yu, M.; Wang, H.; and Shao, L. 2020. Star: A structure and texture aware retinex model. *IEEE Transactions on Image Processing*, 29: 5022–5037.
- Yang, Q.; Wang, S.; and Ahuja, N. 2010. Real-time specular highlight removal using bilateral filtering. In *European conference on computer vision*, 87–100. Springer.
- Ye, G.; Garces, E.; Liu, Y.; Dai, Q.; and Gutierrez, D. 2014. Intrinsic video and applications. *ACM Transactions on Graphics (ToG)*, 33(4): 1–11.
- Yi, R.; Tan, P.; and Lin, S. 2020. Leveraging Multi-View Image Sets for Unsupervised Intrinsic Image Decomposition and Highlight Separation. In *Proceedings of the AAAI Conference on Artificial Intelligence*, volume 34, 12685–12692.
- Yu, Y.; and Smith, W. A. 2019. InverseRenderNet: Learning single image inverse rendering. In *Proceedings of the IEEE/CVF Conference on Computer Vision and Pattern Recognition*, 3155–3164.
- Zhang, Q.; Zhou, J.; Zhu, L.; Sun, W.; Xiao, C.; and Zheng, W.-S. 2021. Unsupervised Intrinsic Image Decomposition using Internal Self-similarity Cues. *IEEE Transactions on Pattern Analysis and Machine Intelligence*.
- Zhang, X.; Ng, R.; and Chen, Q. 2018. Single image reflection separation with perceptual losses. In *Proceedings of the IEEE conference on computer vision and pattern recognition*, 4786–4794.
- Zhao, Q.; Tan, P.; Dai, Q.; Shen, L.; Wu, E.; and Lin, S. 2012. A closed-form solution to retinex with nonlocal texture constraints. *IEEE transactions on pattern analysis and machine intelligence*, 34(7): 1437–1444.
- Zhou, B.; Khosla, A.; Lapedriza, A.; Oliva, A.; and Torralba, A. 2016. Learning deep features for discriminative localization. In *Proceedings of the IEEE conference on computer vision and pattern recognition*, 2921–2929.